

## Energy-Efficient Applications using Surfaces with Special Wettabilities

Kyoo-Chul Park<sup>1,2</sup>, Abhijeet<sup>3</sup>, Wonjae Choi<sup>3\*</sup>

<sup>1</sup>School of Engineering and Applied Sciences, Harvard University, Cambridge, Massachusetts, USA

<sup>2</sup>Wyss Institute for Biologically Inspired Engineering, Harvard University, Cambridge, Massachusetts, USA

<sup>3</sup>Department of Mechanical Engineering, University of Texas at Dallas, USA

\*Corresponding author: Wonjae Choi, Department of Mechanical Engineering, University of Texas at Dallas, USA; E-Mail: wonjae.choi@utdallas.edu

Received Date: February 04, 2014 Accepted Date: March 15, 2014 Published Date: March 18, 2014

Citation: Kyoo-Chul Park, et al. (2014) Energy-Efficient Applications using Surfaces with Special Wettabilities. J Nanotech Smart Mater 1: 1-9

### Abstract

This review focuses on fundamental principles and recently highlighted applications of surfaces with special wettabilities. After briefly introducing the role of surface chemistry and topography on the surface wettabilities, we cover three kinds of functional surfaces whose wettabilities are tailored to improve the energy efficiency of different systems: We first discuss how to use superhydrophobic surfaces to reduce frictional energy dissipation occurring in the water flow on solid surfaces. The next topic is the enhancement of boiling heat transfer, based on surfaces with extreme wettabilities. Finally, we review a bio-inspired surfaces for water collection (e.g., fog harvesting) without active energy input.

### Introduction

This paper reviews recent research on the application of micro- or nanoengineered surfaces that display specially-designed wettabilities. A variety of natural surfaces display such unconventional wettabilities against water – e.g., superhydrophobicity or superhydrophilicity. Several organisms found in nature that have such surfaces include lotus leaves [1], water striders (hitherto superhydrophobic) [2], desert beetles (patterned with regions of different wettabilities) [3], leaves of *Ruellia devosiana* [4], various water plants and moss (superhydrophilic) [5]. Such extreme wetting or non-wetting characteristics attracted both academic and industrial interests, and various research groups have investigated the underlying principles to develop artificial surfaces with different levels of water affinity or repellency [6-10]. The applicability of these synthetic surfaces are extremely wide, ranging from superhydrophilic surfaces displaying antifogging [11] and anti-fouling [12] properties to superhydrophobic surfaces that can prevent wetting [13], corrosion by chemicals [14] and snow adhesion [15]. Furthermore, a surface patterned with regions of different wettabilities can be used as a tool to separate different liquids [16] or to promote self-assembly [17]. Among these various applications, this paper reviews the more recent

applications in three categories that are relevant to energy efficiency: surfaces that can i) reduce drag, ii) facilitate boiling heat transfer, and iii) harvest fog without energy input.

### Extreme Wettabilities

The contact angle (CA) of a water droplet on a surface is commonly used to define wettability of the surface, and a surface is typically classified to be superhydrophilic ( $CA < 10^\circ$ ; see Fig. 1a), hydrophilic ( $CA < 90^\circ$ ), hydrophobic ( $CA > 90^\circ$ ), and superhydrophobic ( $CA > 150^\circ$ ; see Fig. 1b) based on the CA values [18]. This simple definition, sometimes, is not sufficient to explain various wetting phenomena and thus researchers use multiple other metrics including dynamic contact angle, contact angle hysteresis, roll-off angle, and wetting time as complementary measures to quantify wettabilities.

If a surface is smooth and hysteresis-free, the contact angle of a liquid droplet at thermodynamic equilibrium is uniquely determined when the Gibbs free energy consisting of the three interfacial energies ( $\gamma$ ) between solid (s), liquid (l), and vapor (v) phases is minimized. The contact angle in such an energy minimum state is described by the Young's equation: [1]

$$\cos\theta = (\gamma_{sv} - \gamma_{sl}) / \gamma_{lv} \quad (1)$$

, where the equilibrium contact angle  $\theta$  is called as the intrinsic or Young's contact angle. In theory, Eq. 1 can yield extreme  $\theta$  values such as  $0^\circ$  or  $180^\circ$  when the absolute difference between  $\gamma_{sv}$  and  $\gamma_{lv}$  is larger than  $\gamma_{lv}$  (i.e.,  $|\gamma_{sv} - \gamma_{sl}| >$

$\gamma_{lv}$ ). Practically, however, it is rare to observe super hydrophobicity or superhydrophilicity on smooth surfaces because  $\gamma_{sv}$  values fall between 10 mN/m ( $\gamma_{sv} \approx 18$  mN/m for Teflon) to 100 mN/m ( $\gamma_{sv} \approx 300$  mN/m for clean glass, but such a high-energy surface is unstable and becomes readily coated with organic contaminants), causing  $|\gamma_{sv} - \gamma_{sl}|$  to be smaller than the surface tension of water ( $\gamma_{lv} = 72.1$  mN/m).

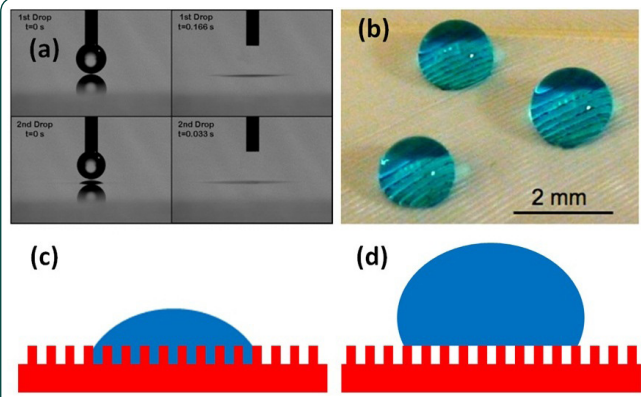


**Figure 1. Wettability of textured surfaces:** (a) Rapid spreading of water droplets on a superhydrophilic surface. Reprinted from reference [11], Copyright 2006, with permission from American Chemical Society. (b) Water droplets on a superhydrophobic duck feather. Reprinted from reference [19]. (c) A schematic illustration of a Wenzel state. In this state, the contacting liquid droplet (represented by blue color) completely fills any gap between protrusions present on the surface (represented by red color). (d) A schematic illustration of a Cassie-Baxter state. In this case the liquid droplet is supported partially on the solid substrate and partially on vapor, forming a solid-liquid-vapor composite interface.

Numerous studies have shown that most naturally superhydrophobic and superhydrophilic surfaces are textured with roughness on multiple scales, e.g., micro- and nanoscales. Such roughness, in conjunction with surface chemistry, can imbue extreme wettabilities to the textured surfaces. Unlike the droplet on a smooth surface, the Gibbs free energy of a water droplet on a rough surface can reach one of two distinct minima, one local and the other global, at the following two configurations [20-21]. In the first case, the free energy reaches its minimum when water penetrates between surface asperities and completely wets the surface (Fig. 1c). In this fully wetted state, the apparent contact angle ( $\theta^*$ ) on the rough surface can be described by the Wenzel relation: [22]

$$\cos\theta^* = r\cos\theta \quad (2)$$

, where  $r$  is the surface roughness defined as the ratio of actual surface area to projected surface area. In this so-called “Wenzel” regime, the intrinsic wettability of the surface is amplified by the surface roughness ( $r$ ), that is, one can make an extremely wetting or non-wetting surface using weakly hydrophilic or hydrophobic material. Indeed, most synthetic surfaces that display superhydrophilicity are based on this principle [11].

Even though one can achieve a high apparent angle Wenzel regime, such regime is not typically used to develop superhydrophobic surfaces because water droplets in the Wenzel regime, even if the apparent contact angle is greater than  $150^\circ$ , do not readily roll-off the surface [23-24]. The reason for this stickiness is that the numerous, fully-wetted surface asperities under the water droplet function as anchors, retarding the receding motion of droplets. Slippery superhydrophobic surfaces emerge when the droplet on

the solid surface reaches its second minimum of free energy, a state in which water does not penetrate into the pores and valleys between surface texture, but is supported partially by vapor. In this regime, water, solid, and vapor form a composite interface – a combination of solid-liquid and liquid-vapor interfaces (Fig. 1d), and the water droplet sits on a carpet of numerous pockets of vapor (or simply air) trapped between surface asperities. The Cassie-Baxter equation describes the apparent contact angle in this composite state as below:[13]

$$\cos\theta^* = \phi_s \cos\theta - 1 + \phi_s \quad (3)$$

, where  $\phi_s$  and  $(1-\phi_s)$  are the areal fractions of solid-liquid and liquid-vapor interfaces. In general, water droplets in this composite Cassie-Baxter regime can easily roll off the surface as long as the fraction  $\phi_s$  is very low, and thus most research on superhydrophobic surfaces exploit this regime [13], [15], [25]. It should be noted that a water droplet in a Cassie-Baxter regime on a textured surface can transition to a Wenzel regime with sufficient pressure perturbations, and thus the robustness of superhydrophobic regime is an important topic in the field.

As we mentioned at the beginning, although Eqs. 2 and 3 can predict the contact angles of droplets in the Wenzel and Cassie-Baxter regimes, the contact angles themselves do not fully characterize various wetting characteristics. Indeed, the energy efficiency of each of all the three applications that we review in this paper is based on at least one more parameter associated with surface wettability: the length scale of surface texture (drag reduction), the combination of regions with different wettabilities (boiling), as well as the advancing and receding contact angles (fog harvesting).

## Drag Reduction

This section focuses on the effect of superhydrophobic surfaces on drag reduction, that is, reducing frictional energy dissipation at the solid-liquid interface. Such solid-water interfaces form, for example, when a solid object is immersed in water, and frictional interactions between the solid and water flow are important at various length scales ranging from submarines (tens of meters) down to microfluidic devices (few microns). For a flow of a viscous Newtonian fluid on a smooth solid surface, the no-slip boundary condition at the interface is widely accepted to be valid as relative motion between the liquid and the solid across the interface can be considered to be negligible [26-29]. This no-slip boundary condition results in the velocity profile of the liquid, relative to the solid, varying from zero up to the velocity of the bulk liquid as shown in Fig. 2a. This velocity gradient leads to a corresponding wall shear stress  $\tau_w = \mu(\partial V_x / \partial Z)_{Z=0}$ , where  $\mu$  is the viscosity of the liquid, and consequently generates the energy dissipation by viscous friction.

Since viscous skin friction is one of the major sources of hydrodynamic drag, there have been numerous studies aimed at designing surfaces that would allow the contacting liquid to slip on the surface and reduce the viscous friction[30-32]. While some research groups investigated the effect of contact angles on the drag reduction[27][33], most recent studies have attempted to utilize the air layer or ‘plastron’ [34][35] entrapped on superhydrophobic surfaces as the lubrication layer to reduce drag. The length scale and topography of the surface texture have been intensively investigated because of

their importance, and some studies even used hierarchical textures[36-43]. These textured surfaces form solid-liquid-air composite interfaces when contacting water, by entrapping numerous pockets of air between their surface textures. Provided that the entrapped air layer is stable against externally imposed pressure differences[44], such surfaces can reduce the frictional energy dissipation associated with viscous flows. Fig. 2b shows one representative configuration of water flow on a non-wetting textured surface. The no-slip boundary condition holds only at the solid-liquid interface, whilst water can freely slip on the liquid-air interface. The resulting wall velocity of water measured at  $z = 0$  (on the top of the textures) becomes significantly greater than zero, i.e.,  $V_w > 0$  [45],[46] on non-wetting textured surfaces. The modification to the resulting velocity profile is commonly represented in terms of a slip coefficient  $\beta$  ( $V_w = \beta \tau_w$ ;  $\tau_w$  is the shear stress at the wall) or a slip length  $b_{\text{slip}}$  ( $V_w = b_{\text{slip}} \gamma_w$ ;  $\gamma_w$  is the shear rate at the wall). For a Newtonian fluid that can be modeled as  $\tau_w = \mu \gamma_w$ , obviously  $\beta = b_{\text{slip}} / \mu$ .

The amount of reported drag reduction greatly varies; for example, Watanabe et al. or Truesdell et al. demonstrated 14% – 20% reduction of hydrodynamic drag in their 16 mm-diameter pipeline or cylindrical rheometer, whose inner surfaces were engineered to be superhydrophobic[36], [43]. On the other hand, other researchers reported substantially smaller drag reduction as well[47]. The main reason for this large variation in the reported drag reduction values is that the amount of drag reduction is proportional not to the slip length itself but to the ratio of the slip length to the thickness of a shear layer[44]. When the thickness of the shear layer is on the order of a centimeter, slip length of tens of microns would not have a practical effect on the amount of drag reduction. Another reason is that, even if a solid surface is superhydrophobic, the slip length can significantly vary depending on the values of two parameters: the solid-liquid areal fraction  $\phi_s$  (see Eq. 3) and the length scale of surface texture[37], [44], [48]. Although water can glide on vapor (or air) pockets entrapped on a superhydrophobic surface, no-slip boundary condition still applies on the tops of solid asperities, greatly reducing the slip length from its potential maximum value (the thickness of the air layer times the ratio between the viscosities of water and air; the ratio is  $40 \sim 60$  at room temperature).

Ybert, et al. [48] developed a mathematical model to predict the slip lengths for liquid flows on different types of surface texture. They used scaling laws to derive generic rules that can estimate the slip length as a function of solid-liquid areal fraction and wave length of two types of superhydrophobic surfaces – surfaces textured with an array of posts or of grates. Later Lee, et al. [37] empirically validated the model (see Fig. 2c, 2d), and Srinivasan, et al. [44] combined the model to suggest that the drag reducing capability of superhydrophobic surfaces is negatively coupled with the stability of the Cassie-Baxter regime. In other words, it can be impractical to develop a superhydrophobic surface that can significantly reduce drag and can be robust against pressure perturbations.

Multiple approaches have been suggested to overcome this limitation. A superhydrophobic surface with an additional level of surface texture – dual-scale texture or re-entrant texture

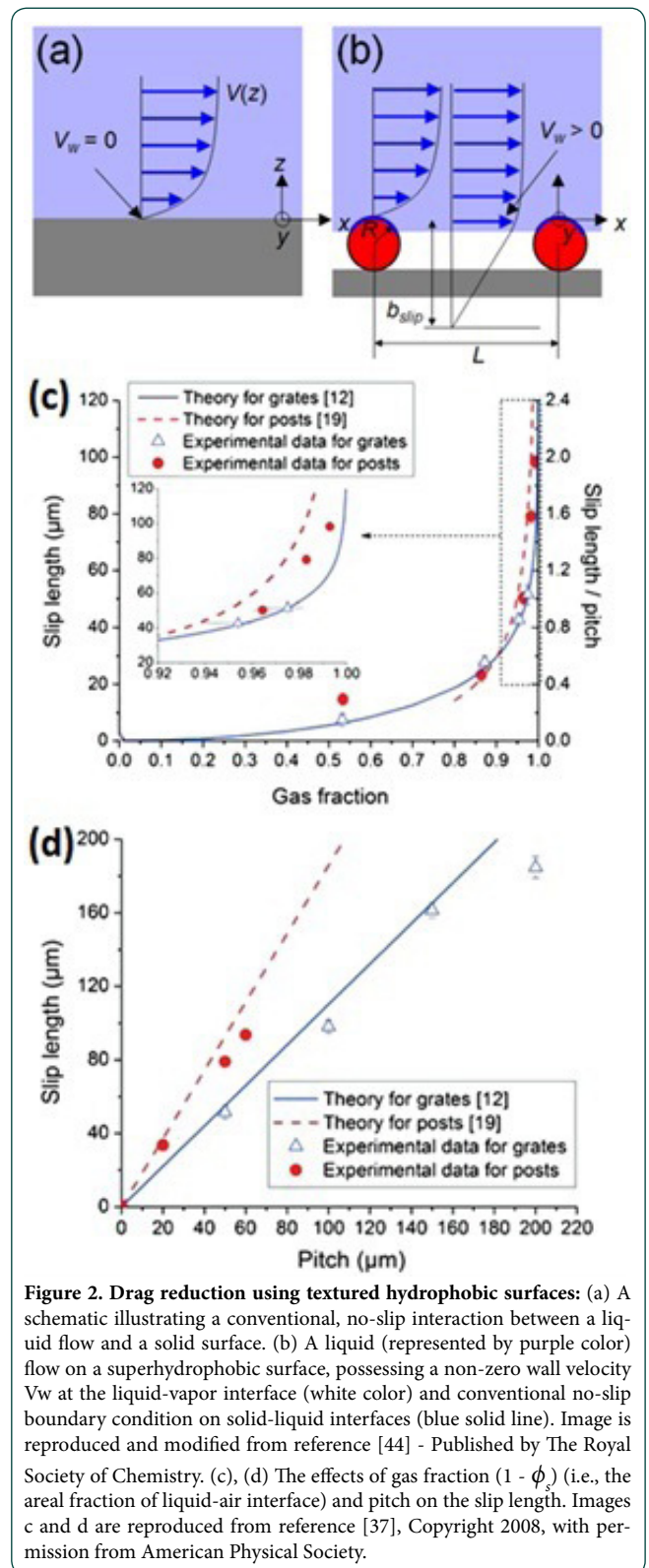


**Figure 2. Drag reduction using textured hydrophobic surfaces:** (a) A schematic illustrating a conventional, no-slip interaction between a liquid flow and a solid surface. (b) A liquid (represented by purple color) flow on a superhydrophobic surface, possessing a non-zero wall velocity  $V_w$  at the liquid-vapor interface (white color) and conventional no-slip boundary condition on solid-liquid interfaces (blue solid line). Image is reproduced and modified from reference [44] - Published by The Royal Society of Chemistry. (c), (d) The effects of gas fraction ( $1 - \phi_s$ ) (i.e., the areal fraction of liquid-air interface) and pitch on the slip length. Images c and d are reproduced from reference [37], Copyright 2008, with permission from American Physical Society.

– was proposed as a solution to increase the resistance against the penetration of water (see Fig. 3a and 3b)[42]. Another research group tried to stabilize the water-vapor meniscus by introducing a feedback channel beneath the superhydrophobic surface as illustrated in Fig. 3c [49]. Alternatively, Shirtcliff et al. suggested that it was possible to achieve a practical drag reduction without a very large slip length, by maintaining the length scale of the flow to be low – e.g., one can readily achieve

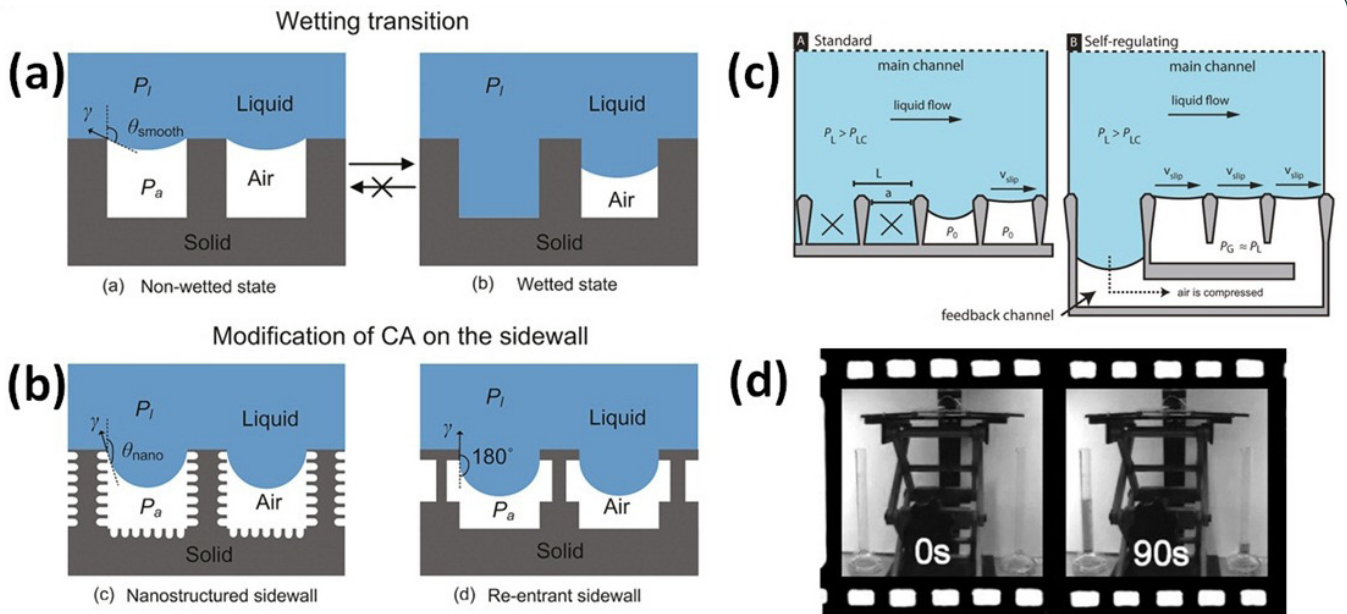


**Figure 3. Surfaces that exhibit significant reduction of drag:** (a) The irreversible transition from the Cassie-Baxter to Wenzel regime occurs when the meniscus of water forms Young's contact angle on the vertical wall of surface texture. (b) Superhydrophobic surfaces with dual-scale texture (left) or re-entrant texture (right) may display higher resistance against the penetration of water as the apparent contact angle on the main asperities can reach as high as  $180^\circ$ . Images in (a) and (b) are reprinted from reference [42], Copyright 2009, with permission from American Chemical Society. (c) The collapse of air pockets due to pressure perturbation (left), which can be prevented by introducing a feedback channel (right). Image is reprinted from reference [49], Copyright 2010, with permission from American Chemical Society. (d) The flow of water through a superhydrophobic (left) and clean, hydrophilic copper tube (right). Water enters from the top through a vertical pipe at the center, splits at the T junction toward the two horizontal pipes. Two graduated cylinders at the bottom collect the discharged water. After 90 seconds, the left cylinder becomes almost half full while the right one remains to be almost empty, indicating that water preferentially flows along the superhydrophobic pipe. Image is reprinted and modified from reference [50], Copyright 2009, with permission from American Chemical Society.

a reasonable reduction of drag in a small pipe (Fig. 3d)[50].

## Boiling Heat Transfer

Boiling has been used in a wide range of industrial systems including heating and cooling facilities, power generators, as well as distillation columns[51], [52]. In most cases, boiling of a liquid (mostly water) is heterogeneous, that is, boiling occurs at the interface between the liquid and the contacting solid surface (e.g., the surface of heaters), not in the bulk liquid itself. The efficacy of boiling heat transfer is thus characterized by the heat transfer coefficient (HTC;  $HTC = q / \Delta T$ ), that is, the ratio between the heat flux  $q$  and the wall superheat ( $\Delta T$ ; the difference between the temperature of the heating surface and the boiling point of the liquid)[53]. Boiling is a heat transfer process with an exceptionally high heat transfer rate (see Fig. 4a to compare the heat flux in the region origin-A and region A-B), because i) the process uses the latent heat associated with the phase transition from the liquid to the vapor state of substance, and ii) rising bubbles from the boiling surface function as mixers, greatly strengthening the convective flow. Boiling process in this highly efficient regime is called as nucleate boiling (region A-C in Fig. 4a).

The HTC associated with a nucleate boiling process changes as a function of wall superheat but the HTC profile can be very different depending on the surface wettability. This is because the boiling process is affected by two phenomena – the rate of nucleation of bubbles on the heating surface, and the rate of their departure[52], [55]. When the heat flux is marginally sufficient to cause the evaporation of

liquid (see region A-B in Fig. 4a), the HTC is mostly determined by the nucleation rate of bubbles. As we discussed at the beginning of the review, hydrophobic or superhydrophobic surfaces repel water and thus they are ideal surfaces to introduce more bubble-nucleation sites on the heating surface. Jo, et al. [54] compared the HTC values for water boiling on smooth hydrophobic and hydrophilic surfaces to find out that the HTC on a hydrophobic surface is significantly higher than that on a hydrophilic surface, as long as the heat flux is low (Fig. 4b; see the region with the wall superheat below 20 K).

When the wall superheat increases, however, the increase of heat flux slows down and eventually reaches an extremum (point C in Fig. 4a) beyond which the heat flux decreases with increasing wall superheat. The heat flux at this extremum is called as the critical heat flux (CHF), and this phenomenon occurs because, as the heat flux increases, the large amount of bubbles nucleating on the heating surface becomes an insulation layer between the liquid and the solid surface. The transition to such a film-boiling regime (between point C and E in Fig. 4a) is due to the following two instabilities: i) the evaporation is so rapid that the liquid cannot rewet the heating surface (Leidenfrost instability)[53], [56], or ii) the viscous friction between the bubbles and the liquid, whose flow directions are toward the opposite, prevents the new bubbles forming on the surface from timely departure (a hydrodynamic instability)[57]. Heat transfer equipment associated with boiling process should operate below its CHF, because film boiling is inherently unstable and thus can lead to an abrupt thermal glitch and eventually the failure of the system. In this high heat flux regime, a hydrophilic or superhydrophilic surface can

be beneficial as they can delay the onset of Leidenfrost instability and thus increase the CHF. The study by Jo, et al. [54] compared also the CHF values on smooth hydrophobic and hydrophilic surfaces (Fig. 4b; see the region with the wall superheat over 20K), and reported that the CHF on a hydrophilic surface is four times as large as that on a hydrophobic surface.

However, the discrepancy between the exceptionally high CHF values reported by these studies and the values predicted by Zuber's model cannot be readily explained. It should be mentioned that, it is relatively straightforward to understand the role of surface wettability on the boiling characteristics when the surface is smooth, as there is only one control parameter (contact angle) that affects boiling.

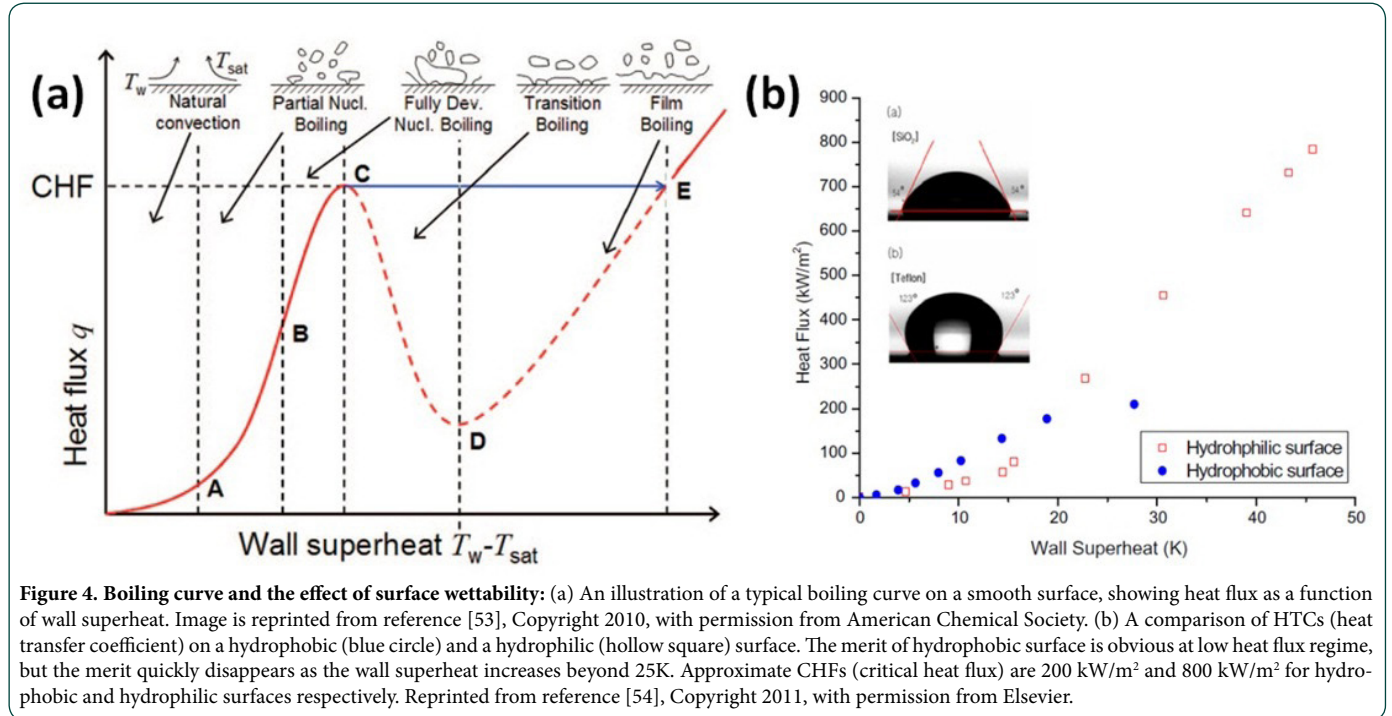


**Figure 4. Boiling curve and the effect of surface wettability:** (a) An illustration of a typical boiling curve on a smooth surface, showing heat flux as a function of wall superheat. Image is reprinted from reference [53], Copyright 2010, with permission from American Chemical Society. (b) A comparison of HTCs (heat transfer coefficient) on a hydrophobic (blue circle) and a hydrophilic (hollow square) surface. The merit of hydrophobic surface is obvious at low heat flux regime, but the merit quickly disappears as the wall superheat increases beyond 25K. Approximate CHFs (critical heat flux) are 200 kW/m<sup>2</sup> and 800 kW/m<sup>2</sup> for hydrophobic and hydrophilic surfaces respectively. Reprinted from reference [54], Copyright 2011, with permission from Elsevier.

Even if one can postpone the Leidenfrost instability by using a hydrophilic surface, boiling ultimately becomes unstable due to the hydrodynamic instability. The strong non-linearity and chaotic nature of boiling makes it impractical to build an accurate model to describe the hydrodynamic instability on a surface. Zuber[57] assumed that the hydrodynamic instability would occur when the liquid and vapor form a Helmholtz instability at the interface, and derived the CHF that can be transferred during boiling on a smooth surface. His model predicted the CHF to be ~110 W/cm<sup>2</sup> for water. The value agrees well with empirical results (see Fig. 4b to find 80 W/cm<sup>2</sup> on a hydrophilic surface).

Recently, however, multiple studies have revealed that, by using textured surfaces, it is possible to increase the CHF significantly beyond the values predicted by Zuber[53], [58], [59], without compromising the HTC values. This is rather counterintuitive because the HTC tends to increase on hydrophobic surfaces while hydrophilic surfaces lead to the higher CHF; in other words, the HTC and CHF are negatively coupled on a smooth surface with a uniform wettability. The researchers suggested that the asperities on a textured solid surface, even when the surface is superhydrophilic, can facilitate nucleation sites. To further exploit this phenomenon, Jo, et al.[54] and Betz, et al.[60], [61] independently developed surfaces with heterogeneous wettabilities; their surfaces possess hydrophobic or superhydrophobic domains to facilitate bubble nucleation, and hydrophilic or superhydrophilic matrix to suppress the Leidenfrost instability (see Fig. 5a).

Superhydrophobic and superhydrophilic surfaces are, on the other hand, textured with numerous surface asperities of different shapes and length scales. The role of these additional complexities is not fully understood. For example, the study by Betz, et al.[61] demonstrated that hydrophobic nucleation sites surrounded by hydrophilic matrix (see Fig. 5a) could enhance both the CHF and HTC values on the surface, but they have not performed a systematic investigation on the quantitative correlation between the boiling characteristics and various geometric parameters such as the spacing or the size of nucleation sites. One postulation that was suggested is that the bubbles forming on nearby nucleation sites tend to mutually interact, affecting the formation of vapor columns (see Fig. 5b). It is possible that this mutual interaction among nucleation sites might suppress the hydrodynamic instability, and further studies on this topic are required.

### Fog Harvesting Surfaces

#### Fog as abundant water source used by animals and plants

The global water crisis threatens more than 20% of human population in arid regions as shown in Fig. 6a.[63], [64] For the recent decades, fog water has emerged as a solution for such water shortage, particularly in some arid regions near ocean, where fog can be abundant despite the scarcity of rainwater.[63], [65] Fog can form, although in lesser quantity, even in desert areas like Namibia and the Saudi Arabian Peninsula and can be used as a supplemental source of water.

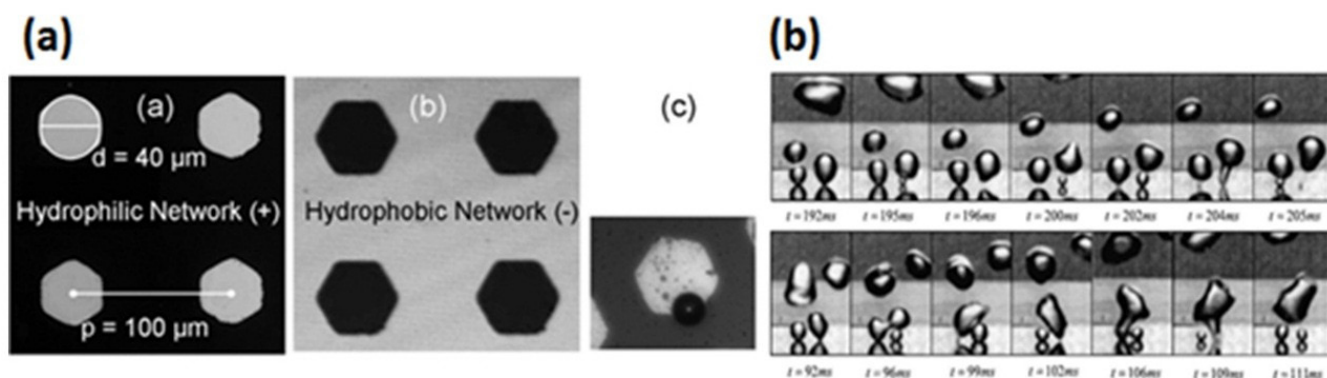


**Figure 5. Surfaces that affect the boiling characteristics:** (a) The first surface (a.a) is patterned with continuous hydrophilic matrix (black) with discrete hydrophobic domains (gray), while the second surface (a.b) is patterned with the opposite polarity. The third panel (a.c) shows the nucleation of bubbles on the patterned surface. Image is reprinted from reference [61], Copyright 2010, with permission from AIP Publishing LLC. (b) The mutual interaction among bubbles nucleating from nearby sites. The figure shows two exemplary patterns - vertical coalescence (top) and declining coalescence (bottom), depending on the spacing between nucleation sites. Image is reproduced from reference [62], Copyright 2003, with permission from Elsevier.

In some cases, the water collected from fog also can be sufficient for plantation and reforestation. Naturally formed fog oasis in Peru and the Fray Jorge fog forest in Chile indicate that fog contains enough water to support vegetation and animal habitat. Fog water supplements the hydrological budget of forests – about 50% of water in Californian redwood tree canopies originate from fog.[66-68] In Chile, Water from fog also provides sufficient amount for reconstruction of ecosystem and even farming[63].

A conventional fog harvester is, simply put, a porous spiderweb-like mesh which collects nearby fog droplets. Compared to fog harvesting that does not require any additional energy input, methods such as multi-stage flash (MSF) process and reverse osmosis (RO) require tremendous amount of electricity;[69], [70] thus MSF and RO cannot be used where electric grid is absent. Economics of fog collections thus compare favorably with MSF and RO desalination technology[70]. Further, fog collectors are easy to construct and maintain, and are not capital intensive, and therefore it is available at a much smaller scale to be used at the village or community level[63], [65].

Before exploring natural and artificial fog harvesting surfaces, it is noteworthy to point out that water harvesting from environmental humidity can be categorized into two types, depending on different water collection mechanisms: (i) fog harvesting that collects airborne water droplets – a group of micrometric airborne water droplets that have already been desalinated by natural solar energy – with diameter ranging from a few micrometers to tens of micrometers and (ii) dew harvesting that collects water vapor (humidity), not droplets, by maintaining the temperature of solid surfaces to be lower than that of ambient humid air. In natural water harvesting process, it is neither necessary nor beneficial to disassemble these two mechanisms because frequently both of them can simultaneously occur (e.g., formation of fog and dew in the early morning). In this review, we will mainly focus on multiple optimization techniques of fog-collecting surfaces based on the role of surface wettability and micro/nanostructures on fog harvesting efficiency. We will briefly discuss a strategy to combine both fog and dew collecting mechanisms in the outlook section.

Airborne water droplets have already been collected by various organisms with specially-designed micro-structured surfaces[3], [71-74] For example, *Stenocara gracilipes*, a beetle living in the Namib desert shown in Fig. 6b, survives by collecting fog on its back that is composed of micrometric hydrophilic islands acting as water collection sites and the surrounding hydrophobic water channels as shown in Fig. 6c.[3] In a similarly arid climate, some plants commonly show a “rosette” shape, a three dimensional structure composed of narrow leaves that directs collected fog toward root[72]. As shown in Figs. 6d-f, a rosette-like microstructure can also be found in the thorns/spines of cactus[73]. The narrow conical microstructure with barbs and grooves on it can transport collected water along the longitudinal direction toward the end with a wider diameter, because such morphology and hydrophilicity cause the meniscus of water droplets to have different curvature (and correspondingly different Laplace pressure) along the axial direction[73]. A similar slender tapered microstructure together with different water wettability is also used to move collected water droplets toward the “knots” from “joints” on spider web threads (Figs. 6g,h)[74].

### Design strategies for artificial fog harvesting surfaces

Inspired by the anisotropic micrometric geometry and water wettability of natural organisms, a number of researchers have studied the strategies for the design and fabrication of artificial fog harvesting surfaces[75-78].

The Namib desert beetle’s back surface with different wetting properties was mimicked by micropipetting hydrophilic materials on highly water repellent surfaces[75], [76]. Simple mist-spraying test showed successful capture of small water droplets on the hydrophilic area, whilst water droplets bounced off superhydrophobic area (Figs. 7a,b) [75]. The water collecting ability of an artificial spider web was also demonstrated by coaxial electrospinning of concentrated polystyrene and dilute poly(methyl methacrylate) solutions as inner and outer solutions, respectively[77]. Further, sponge-like cotton fibers with a polymer layer, whose wettability could be tuned by temperature, exhibited autonomous

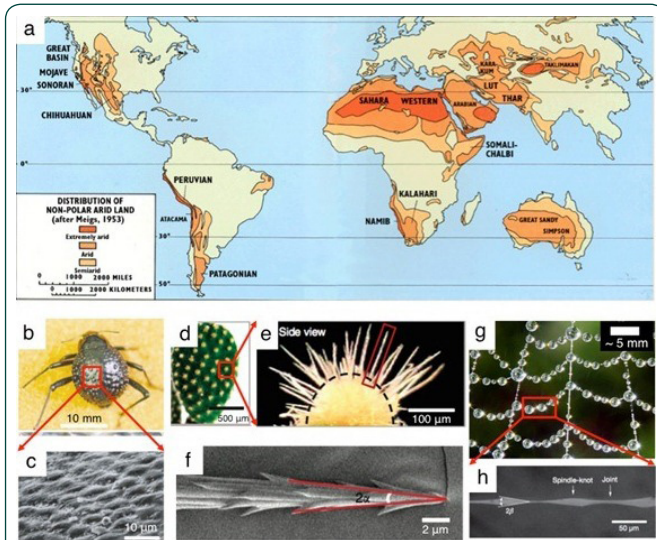


**Figure 6. Overview of arid regions and natural examples of fog harvesting surfaces:** (a) Hyperarid and arid lands, which are deserts, have annually no rainfall and less than 250 mm of rainfall, respectively. In some of hyperarid and arid regions near ocean, abundant fog is one of the most promising sources of water. Reprinted with permission from reference [64]. Source: <http://pubs.usgs.gov/gip/deserts/what/world.html>. (b) The image of the Namib desert beetle and (c) SEM image of its back with hydrophilic bumps surrounded by hydrophobic channels. Reprinted with permission from reference [3], Copyright 2001, Nature Publishing Group. (d-f) Three images of cactus spine structures at different magnifications. Reprinted with permission from reference [73]. Copyright 2012, Nature Publishing Group. (g,h) The droplets formed on spiderweb in early mornings and result from the repeated spindle-knot and joint structures with different wetting characteristics. (g) Image Courtesy of William Lee (h) Reprinted with permission from reference [74]. Copyright 2010, Nature Publishing Group.)

water collection/release mechanism as shown in Figs. 7c-f [77]. The change of extreme wettability is based on the transition of poly(N-isopropylacrylamide), PNIPAAm between hydrophobicity and hydrophilicity across its lower critical solution temperature (LCST), in conjunction with the micro-roughness the polymer layer; the authors demonstrated that the change was repeatable and reversible for many cycles[77].

In practice, simple polyolefin fog collecting meshes have been successfully implemented in the field over many decades in more than 17 countries – United States (California), Chile, Peru, Guatemala, Columbia, Caribbean Islands, Morocco, Spain, Croatia, Eritrea, South Africa, Namibia, Ecuador, Oman, Yemen, UAE, and Nepal[65], [79], [80]. In some regions like El Tofo in Chile, tens of thousands of liters of water were collected per day by dozens of large fog collectors (Fig. 7g)[65]. Based on the numerous studies[81], [82]. on the efficiency of fog collecting meshes, a recent work[83] integrated a systematic analysis of the flow, the mesh geometry (Fig. 7h) and the mesh surface wettability (Figs. 7i,j). The authors proposed a framework that extended the geographic and temporal applicability of the fog collection technology, by revealing the critical influence of surface wettability on the shedding of water droplets deposited on the mesh surface[83]. A surface with a lower difference between advancing and receding contact angles (in other words, contact angle hysteresis)[30] can prevent the clogging problem that significantly lowers fog harvesting efficiency. By understanding the fundamental bulk and interfacial fluid dynamics that control the physics of the fog collection process, they were able to select an

optimal woven design that provided a 500% enhancement in the fog collection efficiency, compared to conventionally-used polyolefin meshes, under mild convective fog conditions[83].

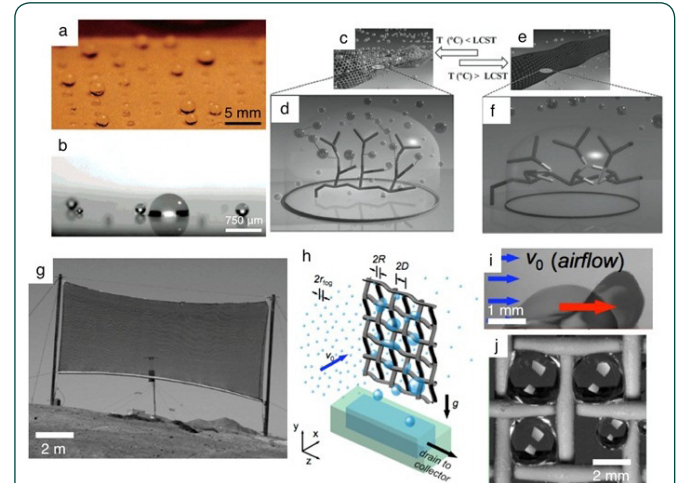


**Figure 7. Artificial fog harvesting surfaces:** (a,b) Water droplets formed by spraying mist on poly(acrylic acid) (PAA) patterned superhydrophobic surfaces that mimic the fog-collecting capabilities of the Namib desert beetle. Reprinted with permission from reference [75]. Copyright 2006, American Chemical Society. (c,d) Illustration of water collection state by hydrogen bonding between molecules of poly(N-isopropylacrylamide) (PNIPAAm) at lower temperature than low critical solution temperature (LCST). Reprinted with permission from reference [77]. Copyright 2013, WILEY-VCH Verlag GmbH & Co. KGaA, Weinheim. (e,f) Illustration of PNIPAAm intermolecular bonds at higher temperature than LCST, resulting in water release (superhydrophobic) state. Reprinted with permission from reference [77]. Copyright 2013, WILEY-VCH Verlag GmbH & Co. KGaA, Weinheim. (g) Image of a large fog collector made of Raschel mesh. (Image Courtesy of Pilar Cereceda) (h) Illustration of fog harvesting mechanism on permeable network of fibers. A portion of small fog droplets coming to the woven mesh structure are captured and deposited droplets are drained downward when gravitational force acting on the deposited droplets exceeds the pinning force that is attributed to water contact angle hysteresis of the fiber surface material. Reprinted with permission from reference [83]. Copyright 2013, American Chemical Society. (i,j) Two distinct factors that reduce the fog collection efficiency – (i) the re-entrainment of collected droplets by air drag force and (j) blockage of the mesh by deposited droplets. These factors are attributed to the wetting characteristics of mesh surface material and can be tuned by the application of surface coating to achieve a higher fog collection efficiency. Reprinted with permission from reference [83]. Copyright 2013, American Chemical Society.

## Perspective / Conclusions

### Drag reduction

It is proven that superhydrophobic surfaces can be used to reduce frictional drag along narrow pipes (e.g., with a diameter of millimeters), as even a very small (e.g.,  $\sim 10 \mu\text{m}$ ) slip length can cause a large difference for the velocity profile in such channels. The commercialization of drag-reducing superhydrophobic surfaces for external flows, however, remains to be challenging. The slip length on a superhydrophobic surface should be at least tens to hundreds of microns to have a noticeable effect on the skin friction for external flows. As we discussed, unfortunately, the robustness of the Cassie-Baxter regime and the slip length are negatively coupled. Surfaces with dual texture seem to be promising as a potential solution to overcome the noted limitation, but even such surfaces will eventually fail unless water is saturated with gas. This is because the inequality between the chemical potentials will cause the gas in the air pocket to diffuse into the bulk water, creating

the pressure difference across the liquid-vapor interface and eventually causing the meniscus bulge into the pores. Such curvature, even if the textured surface can maintain the Cassie-Baxter regime, can compromise the drag reducing ability of superhydrophobic surfaces[84]. As far as the authors know, no ultimate solution for this issue has been reported or suggested.

## Boiling

Unlike the case of drag reduction, surfaces with micro- or nanotextures have already been intensively used to enhance HTC or CHF associated with boiling processes. Most research is based only on the surface wettability – a macroscopic manifestation of numerous asperities and chemical heterogeneities, averaged over spatial domain. There is not, however, sufficient understanding regarding the effect of details, such as the shape and length scale, of surface texture or chemical heterogeneity on the boiling process. We believe that a quantitative model that considers the effect of the geometry of nucleation sites or the influence of the mutual interaction among those sites will allow us to make a significant breakthrough in this area.

## Cost-effective and highly-efficient water collection from thin air

To further reduce the overall cost and increase the amount of collected water, scale-up strategy - a plan for installing a large number of huge fog collectors based on mesh structure – has been tested in Chile[65]. Architectural design for fog harvesters including building exterior and advertisement structures made of permeable materials have been also developed and deployed in these regions. For the next generation of water harvesting surfaces, it can be one of the promising directions to optimize the harvester to efficiently collect both fog [81-83] and dew[85]. For example, the introduction of improved infrared radiation responsive material[86] (to collect dew) to the mesh (a typical fog harvester) may display robust water harvesting efficiency regardless of seasonal or regional humidity conditions.

## Acknowledgments

We thank generous permissions from Prof. Pilar Cereceda and Mr. William Lee for reproducing their images in the figures.

## References

- Barthlott W, Neinhuis C (1997) Purity of the sacred lotus, or escape from contamination in biological surfaces. *Planta* 202: 1-8.
- Gao XF, Jiang L (2004) Water-repellent legs of water striders. *Nature* 432: 36-36.
- Parker AR, Lawrence CR (2001) Water capture by a desert beetle. *Nature* 414: 33-34.
- Koch K, Blecher IC, Koenig G, Kehraus S, Barthlott W (2009) The superhydrophilic and superoleophilic leaf surface of *Ruellia devosi-ana* (Acanthaceae): a biological model for spreading of water and oil on surfaces. *Funct Plant Biol* 36: 339-350.
- Koch K, Barthlott W (2009) Superhydrophobic and superhydrophilic plant surfaces: an inspiration for biomimetic materials. *Philos T R Soc A* 367: 1487-1509.
- Anmin C, Liangliang C, Di G (2007) Fabrication of nonaging superhydrophobic surfaces by packing flowerlike hematite particles. *Appl Phys Lett* 91: 034102.
- Cao L, Hu HH, Gao D (2007) Design and fabrication of micro-textures for inducing a superhydrophobic behavior on hydrophilic materials. *Langmuir* 23: 4310-4314.
- Hoefnagels HF, Wu D, deWith G, Ming W (2007) Biomimetic superhydrophobic and highly oleophobic cotton textiles. *Langmuir* 23: 13158-13163.
- Sun TL, Feng L, Gao XF, Jiang L (2005) Bioinspired surfaces with special wettability. *Acc Chem Res* 38: 644-652.
- Liu XM, He JH (2007) Hierarchically structured superhydrophilic coatings fabricated by self-assembling raspberry-like silica nanospheres. *J Colloid Interface Sci* 314: 341-345.
- Cebeci FC, Wu ZZ, Zhai L, Cohen RE, Rubner MF (2006) Nanoporous-driven superhydrophilicity: A means to create multifunctional antifogging coatings. *Langmuir* 22: 2856-2862.
- Kobayashi M, Terayama Y, Yamaguchi H, Terada M, Murakami D, et al. (2012) Wettability and antifouling behavior on the surfaces of superhydrophilic polymer brushes. *Langmuir* 28: 7212-7222.
- Cassie ABD, Baxter S (1944) Wettability of porous surfaces. *Trans Faraday Soc* 40: 546-551.
- Pan SJ, Kota AK, Mabry JM, Tuteja A (2013) Superomniphobic surfaces for effective chemical shielding. *J Am Chem Soc* 135: 578-581.
- Cao LL, Jones AK, Sikka VK, Wu JZ, Gao D (2009) Anti-icing superhydrophobic coatings. *Langmuir* 25: 12444-12448.
- Kota AK, Kwon G, Choi W, Mabry JM, Tuteja A (2012) Hygro-responsive membranes for effective oil-water separation. *Nat Commun* 3: 1025.
- Kobaku SPR, Kota AK, Lee DH, Mabry JM, Tuteja A (2012) Patterned superomniphobic-superomniphilic surfaces: templates for site-selective self-assembly. *Angew Chem Int Ed* 51: 10109-10113.
- Bhushan B, Jung YC (2007) Wetting study of patterned surfaces for superhydrophobicity. *Ultramicroscopy* 107: 1033-1041.
- Tuteja A, Choi W, Mabry JM, McKinley GH, Cohen RE (2008) Engineering robust omniphobic surfaces. *PNAS* 105: 18200-18205.
- Johnson RE, Dettre RH (1964) Contact angle hysteresis. In *Contact Angle, Wettability and Adhesion*. ACS Advances in Chemistry 112-135.
- Shuttleworth R, Bailey GLJ (1948) The spreading of a liquid over a rough solid. *Discuss Faraday Soc* 3: 16-22.
- Wenzel RN (1936) Resistance of solid surfaces to wetting by water. *Ind Eng Chem* 28: 988-994.
- Bartolo D, Bouamrine F, Verneui É, Buguin A, Silberzan P, et al. (2006) Bouncing or sticky droplets: Impalement transitions on superhydrophobic micropatterned surfaces. *Europhys Lett* 74: 299-305.
- Balu B, Breedveld V, Hess DW (2008) Fabrication of “roll-off” and “sticky” superhydrophobic cellulose surfaces via plasma processing. *Langmuir* 24: 4785-4790.
- Hoefnagels HF, Wu D, de With G, Ming W (2007) Biomimetic superhydrophobic and highly oleophobic cotton textiles. *Langmuir* 23: 13158-13163.
- Stone HA, Lauga E (2007) *Springer handbook of experimental fluid mechanics*. Chapter 19.
- Voronov RS, Papavassiliou DV, Lee LL (2008) Review of fluid slip over superhydrophobic surfaces and its dependence on the contact angle. *Ind Eng Chem Res* 47: 2455-2477.
- Pit R, Hervet H, Leger L (2000) Direct experimental evidence of slip in hexadecane: Solid interfaces. *Phys Rev Lett* 85: 980-983.

- 29) Huang DM, Sendner C, Horinek D, Netz RR, & Bocquet L (2008) Water slippage versus contact angle: A quasiuniversal relationship. *Phys Rev Lett* 101: 226101-226104.
- 30) Quéré D (2008) Wetting and roughness. *Annu Rev Mater Res* 38:71-99.
- 31) Rothstein JP (2010) Slip on superhydrophobic surfaces. *Annu Rev Fluid Mech* 42:89-109.
- 32) McHale G, Newton MI, Shirtcliffe NJ (2010) Immersed superhydrophobic surfaces: Gas exchange, slip and drag reduction properties. *Soft Matter* 6: 714-719.
- 33) Tretheway DC, Meinhart CD (2004) A generating mechanism for apparent fluid slip in hydrophobic microchannels. *Phys Fluids* 16: 1509-1515.
- 34) Shirtcliffe NJ, McHale G, Newton MI, Perry CC, Pyatt FB (2006) Plastron properties of a superhydrophobic surface. *Appl Phys Lett* 89: 2347266-2347267.
- 35) Flynn MR, Bush JWM (2008) Underwater breathing: the mechanics of plastron respiration. *J Fluid Mech* 608: 275-296.
- 36) Watanabe K, Yanuar, Udagawa H (1999) Drag reduction of Newtonian fluid in a circular pipe with a highly water-repellent wall. *J Fluid Mech* 381: 225-238.
- 37) Lee C, Choi CH, Kim CJ (2008) Structured surfaces for a giant liquid slip. *Phys Rev Lett* 101: 064501-064504.
- 38) Ou J, Perot B, Rothstein JP (2004) Laminar drag reduction in microchannels using ultrahydrophobic surfaces. *Phys Fluids* 16: 4635-4643.
- 39) McHale G, Shirtcliffe NJ, Evans CR, Newton MI (2009) Terminal velocity and drag reduction measurements on superhydrophobic spheres. *Appl Phys Lett* 94: 064104-064104-3.
- 40) Choi CH, Ulmanella U, Kim J, Ho CM, Kim CJ (2006) Effective slip and friction reduction in nanogated superhydrophobic microchannels. *Phys Fluids* 18: 087105.
- 41) Salil Gogte, Peter Vorobieff, Richard Truesdell, Andrea Mammoli, Frank van Swol, et al. (2005) Effective slip on textured superhydrophobic surfaces. *Phys Fluids* 17: 051701.
- 42) Lee C, Kim CJ (2009) Maximizing the giant liquid slip on superhydrophobic microstructures by nanostructuring their sidewalls. *Langmuir* 25: 12812-12818.
- 43) Truesdell R, Mammoli A, Vorobieff P, van Swol F, Brinker CJ (2006) Drag reduction on a patterned superhydrophobic surface. *Phys Rev Lett* 97: 044504.
- 44) Srinivasan S, Choi W, Park KC, Shreerang S. Chhatre, Robert E. Cohen, et al. (2013) Drag reduction for viscous laminar flow on spray-coated non-wetting surfaces. *Soft Matter* 9: 5691-5702.
- 45) Bocquet L, Barrat JL (2007) Flow boundary conditions from nano- to micro-scales. *Soft Matter* 3: 685-693.
- 46) Ybert C, Barentin C, Cottin-Bizonne C, Joseph P, Bocquet L (2007) Achieving large slip with superhydrophobic surfaces: Scaling laws for generic geometries. *Phys Fluids* 19: 123601.
- 47) Joseph P, Cottin-Bizonne C, Benoît JM, Ybert C, Journet C, et al. (2006) Slippage of water past superhydrophobic carbon nanotube forests in microchannels. *Phys Rev Lett* 97: 106104.
- 48) Ybert C, Barentin C, Cottin-Bizonne C, Joseph P, Bocquet L (2007) Achieving large slip with superhydrophobic surfaces: Scaling laws for generic geometries. *Phys Fluids* 19: 123601.
- 49) Carlborg CF, van der Wijngaart W (2011) Sustained superhydrophobic friction reduction at high liquid pressures and large flows. *Langmuir* 27: 487-493.
- 50) Shirtcliffe NJ, McHale G, Newton MI, Zhang Y (2009) Superhydrophobic copper tubes with possible flow enhancement and drag reduction. *ACS Appl Mater Interfaces* 1: 1316-1323.
- 51) Patankar NA (2010) Supernucleating surfaces for nucleate boiling and dropwise condensation heat transfer. *Soft Matter* 6: 1613-1620.
- 52) Dhir VK (1998) Boiling heat transfer. *Annu Rev Fluid Mech* 30: 365-401.
- 53) Chen R, Lu MC, Srinivasan V, Wang Z, Cho HH, et al. (2009) Nanowires for enhanced boiling heat transfer. *Nano Lett* 9: 548-553.
- 54) Jo H, Ahn HS, Kang S, Kim MH (2011) A study of nucleate boiling heat transfer on hydrophilic, hydrophobic and heterogeneous wetting surfaces. *Int J Heat Mass Transfer* 54: 5643-5652.
- 55) Dhir VK (2006) Mechanistic prediction of nucleate boiling heat transfer - Achievable or a hopeless task? *J Heat Transfer* 128: 1-12.
- 56) Vakarelski IU, Patankar NA, Marston JO, Chan DYC, Thoroddsen ST (2012) Stabilization of Leidenfrost vapour layer by textured superhydrophobic surfaces. *Nature* 489: 274-277.
- 57) Zuber N (1959) Hydrodynamic aspects of boiling heat transfer. Ph.D. Thesis (University of California at Los Angeles).
- 58) Kim SJ, Bang IC, Buongiorno J, Hu LW (2006) Effects of nanoparticle deposition on surface wettability influencing boiling heat transfer in nanofluids. *Appl Phys Lett* 89: 153107.
- 59) Takata Y, Hidaka S, Masuda M, Ito T (2003) Pool boiling on a superhydrophilic surface. *Int J Energy Res* 27: 111-119.
- 60) Betz AR, Jenkins JR, Kim CJ, Attinger D (2011) Significant boiling enhancement with surfaces combining superhydrophilic and superhydrophobic patterns. *MEMS* 1193-1196.
- 61) Betz AR, Xu J, Qiu HH, Attinger D (2010) Do surfaces with mixed hydrophilic and hydrophobic areas enhance pool boiling? *Appl Phys Lett* 97: 141909-141909.
- 62) Zhang L, Shoji M (2003) Nucleation site interaction in pool boiling on the artificial surface. *Int J Heat Mass Transfer* 46: 513-522.
- 63) Berrahmouni N, Romeo R, McGuire D, Zelaya S, Maselli D, et al. (2011) Highlands and drylands – mountains, a source of resilience in arid regions. Food and Agricultural Organizations for the United Nations and Centre for Development and Environment of the University of Bern.
- 64) U.S. Geological Survey. What is a desert?
- 65) Klemm O, Schemenauer RS, Lummerich A, Cereceda P, Marzol V, et al. (2012) Fog as a fresh-water resource: Overview and perspectives. *Ambio* 41: 221-234.
- 66) Dawson TE (1998) Fog in the California redwood forest: ecosystem inputs and use by plants. *Oecologia* 117: 476-485.
- 67) Limm EB, Simonin KA, Bothman AG, Dawson TE (2009) Foliar water uptake: a common water acquisition strategy for plants of the redwood forest. *Oecologia* 161: 449-459.
- 68) Vasey MC, Loik ME, Parker VT (2012) Influence of summer marine fog and low cloud stratus on water relations of evergreen woody shrubs (*Arctostaphylos*: Ericaceae) in the chaparral of central California. *Oecologia* 170: 325-337.
- 69) Chhatre SS (2013) Designing liquid repellent surfaces for fabrics, feathers, and fog.
- 70) Darwish MA, Al-Najem NM (2000) Energy consumption by multi-stage flash and reverse osmosis desalters. *Appl Therm Eng* 20: 399-416.
- 71) Hamilton WJ, Seely MK (1976) Fog basking by Namib desert bee-

- tle, *Onymacris Unguicularis*. *Nature* 262: 284-285.
- 72) Martorell C, Ezcurra E (2007) The narrow-leaf syndrome: A functional and evolutionary approach to the form of fog-harvesting rosette plants. *Oecologia* 151: 561-573.
- 73) Ju J, Bai H, Zheng Y, Zhao T, Fang R, et al. (2012) A multi-structural and multi-functional integrated fog collection system in cactus. *Nat Commun* 3: 1247 .
- 74) Zheng Y, Bai H, Huang Z, Tian X, Nie FQ, et al. (2010) Directional water collection on wetted spider silk. *Nature* 463: 640-643.
- 75) Zhai L, Michael BC, Fevzi CC, Kim Y, John MM, et al. (2006) Patterned superhydrophobic surfaces: Toward a synthetic mimic of the Namib desert beetle. *Nano Lett* 6: 1213-1217.
- 76) Dorrer C, Rhe J (2008) Mimicking the stenocara beetle-dewetting of drops from a patterned superhydrophobic surface. *Langmuir* 24: 6154-6158.
- 77) Yang H, Zhu H, Hendrix MM, Lousberg NJ, de With G, et al. (2013) Temperature-triggered collection and release of water from fogs by a sponge-like cotton fabric. *Adv Mater* 25: 1150-1154.
- 78) Dong H, Wang N, Wang L, Bai H, Wu J, et al. (2012) Bioinspired electrospun knotted microfibers for fog harvesting. *Chemphyschem* 13: 1153-1156.
- 79) Cereceda P, Larrain H, Osses P, Farías A, Egaña I (2008) The spatial and temporal variability of fog and its relation to fog oases in the Atacama Desert, Chile. *Atmos Res* 87: 312-323.
- 80) Schemenauer RS, Cereceda P (1994) A proposed standard fog collector for use in high-elevation regions. *J Appl Meteorol* 33: 1313-1322.
- 81) Schemenauer RS, Joe PI (1989) The collection efficiency of a massive fog collector. *Atmos Res* 24: 53-69.
- 82) Rivera JD (2011) Aerodynamic collection efficiency of fog water collectors. *Atmos Res* 102: 335-342.
- 83) Park KC, Chhatre SS, Srinivasan S, Cohen RE, McKinley GH (2013) Optimal design of permeable fiber network structures for fog harvesting. *Langmuir* 29: 13269-13277.
- 84) Haase AS, Karatay E, Tsai PA, Lammertink RGH (2013) Momentum and mass transport over a bubble mattress: the influence of interface geometry. *Soft Matter* 9: 8949-8957.
- 85) Lekoucha I, Musellib M, Kabbachia B, Ouazzanib J, Melnytchouk-Milimouk I, et al. (2011) Dew, fog, and rain as supplementary sources of water in south-western Morocco. *Energy* 36: 2257-2265.
- 86) Beysens D, Milimouk I, Nikolayev V, Muselli M, Marcillat J (2003) Using radiative cooling to condense atmospheric vapor: a study to improve water yield. *J Hydrol* 27: 1-11.

**Submit your manuscript to JScholar journals and benefit from:**

- ¶ Convenient online submission
- ¶ Rigorous peer review
- ¶ Immediate publication on acceptance
- ¶ Open access: articles freely available online
- ¶ High visibility within the field
- ¶ Better discount for your subsequent articles

Fostering Scholarly Communication

Submit your manuscript at  
<http://www.jscholaronline.org/submit-manuscript.php>